

Excitation functions of hadronic observables from SIS to RHIC energies*

W. Cassing, E. L. Bratkovskaya and S. Juchem

Institut für Theoretische Physik,
Universität Giessen, 35392 Giessen, Germany

Abstract

We calculate excitation functions for various dynamical quantities as well as experimental observables from SIS to RHIC energies within the HSD transport approach which is based on string, quark, diquark ($q, \bar{q}, qq, \bar{q}\bar{q}$) and hadronic degrees of freedom without including any explicit phase transition to a quark-gluon plasma (QGP). It is argued that the failure of this more 'conventional' approach in comparison to experimental data should indicate the presence of a different phase which might be either attributed to space-time regions of vanishing scalar quark condensate ($\langle q\bar{q} \rangle = 0$) or to the presence of a QGP phase with strongly interacting partons. We study the K/π ratio, the low mass dilepton enhancement in the invariant mass regime from 0.2 – 1.2 GeV as well as charmonium suppression for central Au + Au collisions as a function of the bombarding energy and present predictions for these observables as well as hadron rapidity distributions at RHIC energies. Whereas all observables studied within HSD show smooth increasing/decreasing excitation functions, the experimental K^+/π^+ ratio indicates a maximum at 11 A·GeV (or above) which is interpreted as a signature for a chirally restored phase in the course of the reaction.

PACS: 24.10.-i; 25.75.-q; 11.30.Rd; 13.60.-r

Keywords: Nuclear-reaction models and methods; Relativistic heavy-ion collisions; Chiral symmetries; Meson production

*supported by BMBF and GSI Darmstadt

1 Introduction

The ultimate goal of relativistic nucleus-nucleus collisions is to reanalyze the early 'big-bang' under laboratory conditions and to find the 'smoking gun' for a phase transition from the initial quark-gluon plasma (QGP) to a phase characterized by an interacting hadron gas [1, 2, 3]. Any theoretical approach might describe such a phase transition starting from the partonic side with strongly interacting quarks and gluons [4, 5] or from the hadronic side by involving hadronic degrees of freedom [6, 7], i.e. hadrons with proper self-energies or spectral functions at high baryon density or temperature. It remains to be seen which approach will prove to be more successful, economic and transparent.

Nucleus-nucleus collisions with initial energies per nucleon of $\sqrt{s} = 200$ GeV or ≈ 21.5 A·TeV will be available soon at the Relativistic-Heavy-Ion-Collider (RHIC) in Brookhaven. In central collisions of Au + Au here energy densities above 5 GeV/fm³ are expected such that the critical energy density for a QGP phase should be overcome in considerable space-time volumes where the relevant degrees of freedom are partons (quarks and gluons). Parton cascade calculations have been used so far [4, 8, 9] to estimate the energy densities and particle production yields in violent reactions at $\sqrt{s} = 200$ GeV, an order of magnitude higher than at SPS energies ($\sqrt{s} \approx 20$ GeV). Intuitively one expects that the initial nonequilibrium phase of a nucleus-nucleus collision at RHIC energies should be described by parton degrees of freedom whereas hadrons are only formed (by 'condensation') at a later stage of the reaction which might be a couple of fm/c from the initial contact of the heavy ions. Thus parton cascade calculations – including transition rates from perturbative QCD – should be adequate for all initial reactions involving a large 4-momentum transfer between the constituents since QCD is well tested in its short distance properties. The question, however, remains to which extent the parton calculations can be extrapolated to low Q^2 where hadronic scales become important. As a rough estimate one can employ here the average mass of vector mesons, the nucleon and its first excited state, which gives $Q_{crit}^2 \approx 1$ GeV². On the other hand, using the uncertainty relation this implies time scales of $\Delta t < 0.2$ fm/c = Q_{crit}^{-1} or relative separations of partons $\Delta r < 0.2$ fm, which are small compared to the hadronic size or average life time of the ρ , Δ , etc. in free space or the formation time of hadrons $t_F \approx 0.7 - 0.8$ fm/c as used in the HSD transport approach [10, 11, 12].

Turning the argument around, a nonequilibrium hadronic approach involving a time scale of 0.7-0.8 fm/c cannot tell anything about shorter times because the uncertainty relation does not allow to distinguish states which are separated in mass by less than ≈ 300 MeV = t_F^{-1} , which is the $N - \Delta$ mass difference. Thus one faces the problem that neither the parton description nor a nonequilibrium hadronic model should be valid for times 0.2 fm/c $\leq t \leq 0.7-0.8$ fm/c in individual hadronic reactions, which corresponds to the nonperturbative formation time of the hadronic wavefunction. This regime of the 'soft' QCD physics is presently not well understood and appropriate dynamical models are urgently needed. In the HSD approach these intermediate times are described by color neutral strings, where the leading quarks and 'diquarks' in a baryonic string (or quarks and antiquarks in a mesonic string etc.) are allowed to rescatter again with hadronic cross sections divided by the number of constituent quarks and antiquarks in the hadrons, respectively [12].

Furthermore, the question of chiral symmetry restoration at high baryon density and/or high temperature is of fundamental interest, too [1, 2]. Whereas lattice QCD calculations at

zero baryon chemical potential indicate that a restoration of chiral symmetry goes along with the deconfinement phase transition at some critical temperature T_c , the situation is less clear for finite baryon density where QCD sum rule studies indicate a linear decrease of the scalar quark condensate $\langle \bar{q}q \rangle$ – which is nonvanishing in the vacuum due to a spontaneous breaking of chiral symmetry – with baryon density ρ_B towards a chiral symmetric phase characterized by $\langle \bar{q}q \rangle = 0$. This decrease of the scalar condensate is expected to lead to a change of the hadron properties with density and temperature, i.e. in a chirally restored phase the hadrons might become approximately massless [13] or at least vector and axial vector currents should become equal [14, 15]; the latter implies that the ρ and a_1 spectral functions should become identical. Since the scalar condensate $\langle q\bar{q} \rangle$ is not a direct observable, its manifestations should be found in different hadronic abundancies and spectra.

Nowadays, our knowledge about the hadron properties at high temperature or baryon density is based on heavy-ion experiments from BEVALAC/SIS to SPS energies where hot and dense nuclear systems are produced on a timescale of a few fm/c. As mentioned above, the information from ultrarelativistic nucleus-nucleus collisions at RHIC, i.e. initial $\sqrt{s} = 200$ GeV per nucleon, will be available soon [3]. However, any conclusions about the properties of hadrons in the nuclear environment are based on the comparison of experimental data with nonequilibrium kinetic transport theory [10, 16, 17, 18, 19]. As a genuine feature of transport theories there are two essential ingredients: i.e. the *baryon (and meson) scalar* and *vector self-energies* as well as *in-medium elastic* and *inelastic cross sections* for all hadrons involved. Whereas in the low-energy regime these 'transport coefficients' can be calculated in the Dirac-Brueckner approach starting from the bare nucleon-nucleon interaction [20, 21, 22] this is no longer possible at high baryon density ($\rho_B \geq 2-3\rho_0$) and high temperature, since the number of independent hadronic degrees of freedom increases drastically and the interacting hadronic system should enter a phase with $\langle q\bar{q} \rangle \approx 0$ [13, 14, 23, 24, 25] as mentioned before. As a consequence the hadron self-energies or spectral functions in the nuclear medium will change substantially especially close to the chiral phase transition and transport theoretical studies should include the generic properties of QCD in line with nonperturbative computations on the lattice [26, 27, 28, 29].

In this work we concentrate on excitation functions of hadronic observables from SIS to RHIC energies with the aim to find out optimal experimental conditions to search for 'traditional' phenomena such as strangeness enhancement (Section 3), low mass dilepton enhancement (Section 4) or charmonium suppression in nucleus-nucleus collisions (Section 5). Our studies are performed within the HSD transport approach that has been described in Refs. [11, 12] and been tested for $p + p$, $p + A$ and $A + A$ collisions from the SIS to SPS energy regime [10]. Actual predictions for hadron rapidity spectra and J/Ψ suppression will be presented in Section 6 while Section 7 concludes the study with a summary.

2 Theoretical considerations

In this Section we briefly recall the ingredients of the covariant transport theory, that has been denoted as **H**adron-**S**tring-**D**ynamics (HSD) [11], which formally can be written as a coupled set of transport equations for the phase-space distributions $f_h(x, p)$ of hadron h

[11, 30, 31], i.e.

$$\begin{aligned}
& \left\{ \left(\Pi_\mu - \Pi_\nu \partial_\mu^p U_h^\nu - M_h^* \partial_\mu^p U_h^S \right) \partial_x^\mu + \left(\Pi_\nu \partial_\mu^x U_h^\nu + M_h^* \partial_\mu^x U_h^S \right) \partial_p^\mu \right\} f_h(x, p) \\
& = \sum_{h_2 h_3 h_4 \dots} \int d^2 d^3 d^4 \dots [G^\dagger G]_{12 \rightarrow 34 \dots} \delta_\Gamma^4 (\Pi + \Pi_2 - \Pi_3 - \Pi_4 \dots) \\
& \times \left\{ f_{h_3}(x, p_3) f_{h_4}(x, p_4) \bar{f}_h(x, p) \bar{f}_{h_2}(x, p_2) \right. \\
& \left. - f_h(x, p) f_{h_2}(x, p_2) \bar{f}_{h_3}(x, p_3) \bar{f}_{h_4}(x, p_4) \right\} \dots \quad .
\end{aligned} \tag{1}$$

In Eq. (1) $U_h^S(x, p)$ and $U_h^\mu(x, p)$ denote the real part of the scalar and vector hadron self-energies, respectively, while $[G^\dagger G]_{12 \rightarrow 34 \dots} \delta_\Gamma^4 (\Pi + \Pi_2 - \Pi_3 - \Pi_4 \dots)$ is the 'transition rate' for the process $1+2 \rightarrow 3+4+\dots$ which is taken to be on-shell in the semiclassical limit adopted. The hadron quasi-particle properties in (1) are defined via the mass-shell constraint [31],

$$\delta(\Pi_\mu \Pi^\mu - M_h^{*2}) \quad , \tag{2}$$

with effective masses and momenta (for a hadron of bare mass M_h and momentum p^μ) given by

$$\begin{aligned}
M_h^*(x, p) & = M_h + U_h^S(x, p) \\
\Pi^\mu(x, p) & = p^\mu - U_h^\mu(x, p) \quad ,
\end{aligned} \tag{3}$$

while the phase-space factors

$$\bar{f}_h(x, p) = 1 \pm f_h(x, p) \tag{4}$$

are responsible for fermion Pauli-blocking or Bose enhancement, respectively, depending on the type of hadron in the final/initial channel. The dots in Eq. (1) stand for further contributions to the collision term with more than two hadrons in the final/initial channels. The transport approach (1) is fully specified by $U_h^S(x, p)$ and $U_h^\mu(x, p)$ ($\mu = 0, 1, 2, 3$), which determine the mean-field propagation of the hadrons, and by the transition rates $G^\dagger G \delta^4(\dots)$ in the collision term, that describe the scattering and hadron production/absorption rates.

In Ref. [11] the scalar and vector mean-fields U_h^S and U_h^μ have been determined in the mean-field limit from an effective hadronic Lagrangian density \mathcal{L}_H that has been fitted to the equation of state of nucleonic matter as resulting from the Nambu-Jona-Lasinio (NJL) model. Without going through the arguments again we show in Fig. 1 the nucleon scalar (U_S) and negative vector potential ($-U_0$) as a function of the nuclear density ρ and relative momentum \mathbf{p} of the nucleon with respect to the nuclear matter rest frame. Whereas the vector potential increases practically linearly with density (at low momentum \mathbf{p}) the scalar potential saturates with density such that the nucleon effective mass $M^* = M_0 + U_S$ almost drops to zero for $\rho \geq 0.6 \text{ fm}^{-3}$. Both potentials decrease rather fast in magnitude with momentum \mathbf{p} and practically vanish above a few GeV/c.

In Fig. 2 the real part of the potential

$$U_{SEP} = U_0(\rho_0, \mathbf{p}) + \sqrt{\mathbf{p}^2 + (M_N + U_S)^2} - \sqrt{\mathbf{p}^2 + M_N^2} \tag{5}$$

is shown again as a function of ρ and \mathbf{p} . Whereas we see a net attraction for momenta $|\mathbf{p}| \leq 0.5 \text{ GeV}/c$ up to densities of $\approx 0.3 \text{ fm}^{-3}$, the net potential becomes repulsive for higher

momenta, reaches a maximum repulsion at $|\mathbf{p}| \approx 1 \text{ GeV}/c$ and then drops again with $|\mathbf{p}|$. We mention that at density ρ_0 the potential U_{SEP} compares well with the potential from the data analysis of Hama et al. [32] as well as Dirac-Brueckner computations from [21] up to a kinetic energy E_{kin} of 1 GeV [11]. The formula (5) reduces to the familiar expression for the Schroedinger equivalent potential (Eq. (3.16) of Ref. [10]) in the low density limit.

In our transport calculations we include nucleons, Δ 's, $N^*(1440)$, $N^*(1535)$, Λ , Σ and Σ^* hyperons, Ξ 's and Ω 's as well as their antiparticles. In a first approximation we assume here that all baryons (made out of light (u, d) quarks) have the same scalar and vector self-energies as the nucleons while the hyperons pick up a factor $2/3$ according to the light quark content and Ξ 's a factor of $1/3$, respectively.

In the HSD approach the high energy inelastic hadron-hadron collisions are described by the FRITIOF model [33], where two incoming hadrons emerge the reaction as two excited color singlet states, i.e. 'strings'. According to the Lund model [33] a string is characterized by the leading constituent quarks of the incoming hadron and a tube of color flux is supposed to be formed connecting the rapidly receding string-ends. In the HSD approach baryonic ($qq - q$) and mesonic ($q - \bar{q}$) strings are considered with different flavors ($q = u, d, s$). In the uniform color field of the strings virtual $q\bar{q}$ or $qq\bar{q}\bar{q}$ pairs are produced causing the tube to fission and thus to create mesons or baryon-antibaryon pairs. The production probability P of massive $s\bar{s}$ or $qq\bar{q}\bar{q}$ pairs is suppressed in comparison to light flavor production ($u\bar{u}$, $d\bar{d}$) according to a Schwinger-like formula [34]

$$\frac{P(s\bar{s})}{P(u\bar{u})} = \gamma_s = \exp\left(-\pi \frac{m_s^2 - m_q^2}{2\kappa}\right), \quad (6)$$

with $\kappa \approx 1 \text{ GeV}/\text{fm}$ denoting the string tension. Thus in the Lund string picture the production of strangeness and baryon-antibaryon pairs is controlled by the constituent quark and diquark masses. Inserting the constituent quark masses $m_u = 0.3 \text{ GeV}$ and $m_s = 0.5 \text{ GeV}$ a value of $\gamma_s \approx 0.3$ is obtained. While the strangeness production in proton-proton collisions at SPS energies is reasonably well reproduced with this value, the strangeness yield for $p + \text{Be}$ collisions at AGS energies is underestimated by roughly 30% (cf. [12]). For that reason the relative factors used in the HSD model are [12]

$$u : d : s : uu = \begin{cases} 1 : 1 : 0.3 : 0.07 & , \text{ at SPS to RHIC energies} \\ 1 : 1 : 0.4 : 0.07 & , \text{ at AGS energies,} \end{cases} \quad (7)$$

with a linear transition of the strangeness suppression factor $\gamma_s = s : u$ as a function of \sqrt{s} in between.

Additionally a fragmentation function $f(x, m_t)$ has to be specified, which is the probability distribution for hadrons with transverse mass m_t to acquire the energy-momentum fraction x from the fragmenting string,

$$f(x, m_t) \approx \frac{1}{x} (1-x)^a \exp\left(-bm_t^2/x\right), \quad (8)$$

with $a = 0.23$ and $b = 0.34 \text{ GeV}^{-2}$ [12].

We recall that the LUND model [33] includes partonic diffractive scattering and mini-jet production as well [35]. The latter phenomena are not important at SPS energies and below, however, become appreciable at RHIC energies. In this respect the HSD approach

dynamically also includes the hard partonic processes as far as quarks and antiquarks are involved. However, it does not employ hard gluon-gluon processes beyond the level of 'string phenomenology'. This has to be kept in mind with respect to the predictive power of the model at RHIC energies and beyond.

The medium modifications due to the hadron self-energies, furthermore, require to introduce some conserving approximations in the collision terms in line with the modified quasi-particle properties. Since these in-medium modifications – related to 'low momentum physics' – are not of primary interest in this study we discard an explicit discussion here and refer the reader to Ref. [11].

2.1 The scalar condensate

The scalar quark condensate $\langle q\bar{q} \rangle$ is viewed as an order parameter for the restoration of chiral symmetry at high baryon density and temperature. A model independent relation for the scalar quark condensate at finite (but small) baryon density and temperature has been given by Drukarev and Levin [36], i.e

$$\frac{\langle q\bar{q} \rangle}{\langle q\bar{q} \rangle_V} = 1 - \frac{\rho_S}{f_\pi^2 m_\pi^2} \left[\Sigma_\pi + m_\pi \frac{d}{dm} \left(\frac{E(\rho)}{A} \right) \right], \quad (9)$$

where $\langle q\bar{q} \rangle_V$ denotes the vacuum condensate, $\Sigma_\pi \approx 45$ MeV is the pion-nucleon Σ -term, f_π and m_π the pion decay constant and pion mass, respectively, while $E(\rho)/A$ is the binding energy per nucleon. Since for low densities the scalar density ρ_S in (9) may be replaced by the baryon density ρ_B , the change in the scalar quark condensate starts linearly with ρ_B and is reduced by a factor 1/3 at saturation density ρ_0 . A simple linear extrapolation then would indicate that at $\rho_B \approx 3\rho_0$ a restoration of chiral symmetry might be achieved in heavy-ion collisions.

A reasonable estimate for the scalar condensate in dynamical calculations has been suggested by Friman et al. [37],

$$\frac{\langle q\bar{q} \rangle}{\langle q\bar{q} \rangle_V} = 1 - \frac{\Sigma_\pi}{f_\pi^2 m_\pi^2} \rho_S - \sum_h \frac{\sigma_h \rho_S^h}{f_\pi^2 m_\pi^2}, \quad (10)$$

where σ_h denotes the σ -commutator of the relevant mesons h . For pions and mesons made out of light quarks and antiquarks we use $\sigma_h = m_\pi/2$ whereas for mesons with a strange (antistrange) quark we adopt $\sigma_h = m_\pi/4$ according to the light quark content. Within the same spirit the Σ -term for hyperons is taken as $2/3 \Sigma_\pi \approx 30$ MeV while for Ξ 's we use $1/3 \Sigma_\pi \approx 15$ MeV.

The scalar density of mesons (of type h) is given by

$$\rho_S^h = \frac{(2s+1)(2t+1)}{(2\pi)^3} \int d^3\mathbf{p} \frac{m_h}{\sqrt{\mathbf{p}^2 + m_h^2}} f_h(\mathbf{r}, \mathbf{p}; t), \quad (11)$$

with f_h denoting the meson phase-space distribution of species h . In (11) s, t denote the spin and isospin quantum numbers, respectively. We note that the scalar density of baryons is calculated in line with (11) by replacing the mass and momentum by the effective quantities in (3).

The actual numerical result for the space-time dependence of the scalar condensate (10) is shown in Figs. 3 and 4 for central Au + Au collisions at 6 A·GeV and 20 A·GeV, respectively. Here the condensate is divided by the vacuum condensate $\langle q\bar{q} \rangle_V$ such that the nonperturbative vacuum is characterized by a value of 1. Furthermore, the z -direction has been stretched by the Lorentz-factors γ_{cm} to compensate for Lorentz contraction, while negative numerical values for the condensate have been suppressed. According to (9), (10) the scalar condensate is reduced inside the approaching nuclei by about 35%; this reduction becomes more pronounced when the nuclei achieve full overlap. As seen from Fig. 3 already at 6 A·GeV there is a substantial space-time region of vanishing scalar condensate for $6 \text{ fm}/c \leq t \leq 13 \text{ fm}/c$, where the conventional hadronic picture is not expected to hold anymore. The space-time volume of vanishing quark condensate slightly increases for 20 A·GeV (Fig. 4), however, the increase is only moderate and resembles very much the situation for the space-time integral of high density baryon matter (cf. Fig. 1 in Ref. [38]).

We mention that at higher bombarding energies the 4-volume ($x = (t, \mathbf{r})$)

$$V(\alpha) = \int d^3\mathbf{r}dt \Theta\left(\alpha - \frac{\langle q\bar{q} \rangle_x}{\langle q\bar{q} \rangle_V}\right), \quad (12)$$

that counts the fraction of the scalar condensate below the value of α ($0 \leq \alpha \leq 0.3$) is essentially determined by the pion density whereas below about 20 A·GeV the dominant contribution stems from the baryons (cf. also Ref. [37]). Since the pion density can be considered as a measure of the vacuum 'temperature', a chiral order transition below about 20 A·GeV is dominated by the baryon density while especially at SPS or even RHIC energies a chiral order transition is due to 'temperature'.

The question now arises, if there are proper experimental observables that allow to trace down such type of phase transition (or cross over). When gating on central collisions of Au + Au (or Pb + Pb) such phenomena should show up in their excitation functions. We note that in a pure hadronic transport approach we expect a smooth behaviour of practically all observables with bombarding energy due to an increase of thermal excitation energy. This is not so obvious for the HSD approach where a gradual transition from hadronic excitations to strings and quark (or diquark) degrees of freedom is involved. In fact, in Ref. [39] it has been claimed that the excitation function of transverse and elliptic proton flow together with the transverse p_t spectra of protons suggest a transition from *hadron* to *string* matter at about 5 A·GeV. Here, however, we concentrate on meson abundancies and spectra and refer the reader to Ref. [39] for the collective dynamical aspects and to Ref. [40] for the thermal properties of the theory that involves a limiting ('Hagedorn') temperature of $T_S \approx 150 \text{ MeV}$ due to the continuum string excitations.

3 Meson production

To present a general overview on the meson abundancies in nucleus-nucleus collisions we show in Fig. 5 the meson multiplicities for central collisions of Au + Au from SIS to RHIC energies. All multiplicities for π^+ , η , K^+ , K^- , ϕ as well as J/Ψ mesons show a monotonic increase with bombarding energy which is only very steep at 'subthreshold' energies, i.e. at bombarding energies per nucleon below the threshold in free space for NN collisions. At higher bombarding energies the meson abundancies group according to their quark content,

i.e. the multiplicities are reduced (relative to π^+) by about a factor of 4–5 for a strange quark, a factor of ≈ 50 for $s\bar{s} \equiv \phi$ and a factor of $\approx 2 \cdot 10^5$ for $c\bar{c} \equiv J/\Psi$. We mention that in these calculations the meson rescattering and reabsorption processes have been taken into account; this reduces the J/Ψ cross section at RHIC energies by about a factor of 10 (cf. Section 5). At 'subthreshold' energies the ϕ multiplicity turns out to be almost the same as the antikaon multiplicity, but then rises less steeply with bombarding energy. Apart from the ϕ excitation function – that still has to be controlled experimentally – we thus find no pronounced change in the shape of the meson abundancies up to RHIC energies where data are expected to come up soon.

We recall that our investigations on strangeness production up to 2 A·GeV [41, 42] have given some evidence for attractive antikaon potentials in the medium while for kaons only a very moderate repulsive potential was suggested [42]; η mesons apparently do not show sensible in-medium effects according to the studies in Ref. [43, 44] in comparison to the available experimental spectra. At AGS and SPS energies, on the other hand, the potential effects on kaon and antikaon abundancies have been found to be only very low [10] such that meson potentials have been discarded in Fig. 5 for the overview.

Since the meson abundancies show no sudden change in the excitation function, we turn to particle ratios. Here strangeness enhancement has been suggested for more than 2 decades to possibly qualify as a sensible probe for a QGP phase (cf. Ref. [45] for a recent overview). Here we examine the K^+/π^+ ratio at midrapidity in central Au + Au (or Pb + Pb) collisions where experimental data are now available from SIS to SPS energies [45, 46, 47]. We recall that detailed comparisons of pion and kaon rapidity distributions and transverse momentum spectra to the available data have been presented in Refs. [10, 12] such that we directly can continue with the corresponding excitation function.

In order to discuss the strangeness production over the complete energy range from SIS to RHIC energies we show in Fig. 6 the calculated K^+/π^+ ratio at midrapidity ($-0.5 \leq y_{cm} \leq 0.5$) for central Au + Au collisions in comparison to the experimental data. This ratio experimentally is substantially lower at SPS energies ($\approx 13.5\%$) compared to AGS energies ($\approx 19\%$). At SPS energies this ratio is only enhanced by a factor 1.75 for central Pb + Pb collisions relative to p + p reactions and has to be compared to the factor ≈ 3 at AGS. Such a decrease of the scaled kaon yield from AGS to SPS energies is not described by the HSD transport model (without kaon self-energies) which shows a monotonic increase with bombarding energy similar to pp reactions (open circles). Furthermore, the higher temperatures and particle densities at SPS energies tend to enhance the K^+/π^+ yield closer to its thermal equilibrium value of $\approx 20 - 25\%$ [48] at chemical freezeout and temperatures of $T \approx 150$ MeV.

Our findings have to be compared to results obtained by other microscopic approaches. Here only the RQMD model very recently [49] provides a study partly comparable to that of Ref. [12], however, excluding p + A reactions to control the amount of K^+ production by rescattering. Whereas kaon production in p + p reactions is comparable to our results in [12] (input of the transport model), the RQMD model yields a higher K^+/π^+ ratio in Au + Au, Pb + Pb collisions at all energies due to a higher kaon yield from rescattering. The latter can be attributed to 'high mass strange resonances' that have been incorporated to describe the low energy kaon production via resonance production and decay [50] (s-channels). Since these 'high mass resonances' can be repopulated in resonance-resonance scattering, a rather

high \sqrt{s} is concentrated in a single degree of freedom for a short time. Such 'hot spots' then lead to a higher K^+/π^+ ratio in A + A reactions especially at AGS energies. While the K^+/π^+ ratio can be reasonably described at AGS energies in Au + Au reactions, this ratio is overestimated significantly at SPS energies (cf. Fig. 4 of Ref. [49]). Thus also the RQMD model does not describe the relative decrease of the K^+/π^+ ratio from 11 A·GeV to 160 A·GeV. The results of the RQMD calculations at SIS energies are not known to the authors.

4 Dilepton production

Electromagnetic decays to virtual photons (e^+e^- or $\mu^+\mu^-$ pairs) have been suggested long ago to serve as a possible signature for a phase transition to the QGP [51, 52, 53, 54, 55] or to be an ideal probe for vector meson spectroscopy in the nuclear medium. As pointed out in Refs. [15, 56] the isovector current-current correlation function is proportional to the imaginary part of the ρ -meson propagator and also to the dilepton invariant mass spectra. Dileptons are particularly well suited for an investigation of the violent phases of a high-energy heavy-ion collision because they can leave the reaction volume essentially undistorted by final-state interactions. Indeed, the dilepton studies in heavy-ion collisions by the DLS Collaboration at the BEVALAC [57] and by the CERES [58, 59], HELIOS [60, 61], NA38 [62] and NA50 Collaborations [63] at SPS energies have found a vivid interest in the nuclear physics community.

We recall that the question of chiral symmetry restoration does not necessarily imply that vector meson masses have to drop with baryon density or temperature [64]. Actually, chiral symmetry restoration (ChSR) only demands that the isovector current-current correlation function and the axial vector current-current correlation function (dominated by the chiral partner of the ρ , the a_1 -meson) should become identical at high ρ_B or temperature T , respectively, because there should be no more differences between left- and right-handed particles or equivalently vector and axial vector currents [15, 64]. Thus also a strong broadening of the ρ - as well as the a_1 -spectral function and their mixing in the medium [65, 66, 67, 68] can be considered as a signature for ChSR which, however, is not easy to detect experimentally.

In Ref. [10] we have demonstrated that the present experimental data on the low mass dilepton enhancement at SPS energies can be described equally well within the 'dropping ρ -mass' scenario as well as within the 'melting' ρ picture, which implies a large spreading in mass of the ρ spectral function due to its couplings to baryons and/or mesons. The situation at SIS/BEVALAC energies is more 'puzzling' since here the low mass dilepton enhancement is neither described in the dynamical spectral function approach [44] nor in the 'dropping mass' scheme [69], though the pp dilepton data from the DLS collaboration [70] are reproduced within the known sources rather well from 1 – 5 GeV bombarding energy [71, 72]. In short, the dynamical origin of the low mass dilepton enhancement is not yet understood.

Here we propose to investigate the excitation function of low mass dilepton enhancement in central Au + Au collisions. As discussed in Refs. [10, 68] this excess of dileptons is most probably due to the isovector (ρ) channel, i.e. the imaginary part of the isovector current-current correlation function which, however, mixes with the axial vector current-current

correlation function at finite temperature and baryon density [15, 68].

Since the ρ -meson spectral function is of primary interest, it is important to have some information about the actual baryon densities that the ρ -meson experiences during its propagation and decay in central Au + Au collisions. This information is displayed in Fig. 7 – as resulting from the HSD transport calculation – for central reactions at 2, 5, 10, 20, 40 and 160 A·GeV. Here the meson-baryon production channels and baryon-baryon production channels are summed up by the solid lines and denoted as $(\pi B \rightarrow \rho, BB \rightarrow \rho)$. The meson-meson production channels such as $\pi\pi \rightarrow \rho, a_1 \rightarrow \pi\rho$ etc. are summed up in the dashed histograms indicated as $\pi\pi \rightarrow \rho$ according to the dominating channel. We find that especially the initial BB production channels produce ρ -mesons at very high densities close to $2 \rho_0 \gamma_{cm}$ where γ_{cm} is the Lorentz factor in the cms. However, these production channels are much less abundant than the meson-meson channels which extend over a larger time span (for the heavy system Au + Au) and essentially occur at much lower baryon density, respectively. This effect becomes even more pronounced with increasing bombarding energy, i.e. 40 – 160 A·GeV, where most of the ρ -mesons are produced at baryon densities below $2 \rho_0$. Since in Fig. 7 the relative abundancy of ρ -mesons is displayed as a function of the baryon density at the production (formation) point, the time averaged value of the density is even lower due to a fast expansion of the hadronic fireball. Thus to probe on average high baryon densities by ρ -mesons one should step down in energy to 2 – 5 A·GeV in order to optimize effects due to the coupling to baryons.

A general overview of dilepton mass spectra in central ($b=2$ fm) Au + Au collisions from 2 A·GeV to 21.5 A·TeV is presented in Fig. 8, where the upper part corresponds to the case of vacuum spectral functions for all mesons (cf. Fig. 8.20 of Ref. [10]), while the lower part is calculated by employing the ρ spectral function from Rapp et al. [67, 73]. Whereas for the free meson spectral function one observes essentially an increase of the dilepton production channels with bombarding energy without any substantial change in the spectral shape (except for an increasing peak from the ϕ ; cf. Fig. 5), the in-medium calculations yield almost exponential mass spectra above $M \geq 0.4$ GeV with small peaks from vacuum ω and ϕ decays at $M \approx 0.78$ GeV and 1.02 GeV.

We mention that for the vacuum spectral functions (upper part of Fig. 8) the shape of the dilepton spectra (for $M_{e^+e^-} \geq 0.15$ GeV) is due to the superposition of η, η', ω and a_1 Dalitz decays and direct vector meson decays (ρ, ω, ϕ), where all mesons may also be produced in meson-baryon and meson-meson collisions. The increase in dilepton yield (for $M_{e^+e^-} \geq 0.15$ GeV) with bombarding energy thus is due to an enhanced production of $\eta, \eta', \rho, \omega, \phi, a_1$ mesons. Their relative abundance from SIS to RHIC energies does not scale directly with the charged particle multiplicity which is dominated by protons, π^\pm and K^\pm (cf. Fig. 5). However, above about 50 – 100 A·GeV the meson ratios do not change very much (cf. Figs. 5,6) while the charged particle multiplicity becomes dominated by π^\pm and K^\pm . Thus from SPS to RHIC energies the low mass dilepton yield should approximately be proportional to the charged particle multiplicity, too.

The relative change in the dilepton spectra is quantitatively displayed in Fig. 9 – again for central ($b=2$ fm) collisions of Au + Au – for the case of free meson spectral functions (solid lines) and the spectral function from Rapp et al. [67, 73] (dashed lines). In line with the discussion above the most prominent spectral changes are expected at rather low bombarding energies from 2–10 A·GeV, where the enhancement in the invariant mass range

from 0.3–0.6 GeV is about a factor of 4. Note that the ω and ϕ vacuum decays show clear peaks on top of the ‘exponential’ continuum, which will have to be identified experimentally. We mention that in all our calculations we have incorporated an experimental (‘optimistic’) mass resolution of $\Delta M = 10$ MeV for the dilepton invariant mass.

5 Charmonium production and suppression

Matsui and Satz [74] have proposed that a suppression of the J/Ψ yield in ultra-relativistic heavy-ion collisions is a plausible signature for the formation of the quark-gluon plasma because the J/Ψ should dissolve in the QGP due to color screening. This suggestion has stimulated a number of heavy-ion experiments at CERN SPS to measure the J/Ψ via its dimuon decay. Indeed, these experiments have shown a significant reduction of the J/Ψ yield when going from proton-nucleus to nucleus-nucleus collisions [62]. Especially for Pb + Pb at 160 A·GeV an even more dramatic reduction of J/Ψ has been reported by the NA50 Collaboration [63, 75, 76].

To interpret the experimental results, various models based on J/Ψ absorption by hadrons have been also proposed (cf. Refs. [10, 77, 78] for recent reviews) that do not involve the assumption of a QGP phase transition. The role of comover dissociation is presently again heavily debated [5, 78] especially since theoretical calculations for J/Ψ -meson dissociation cross sections differ by up to a factor of 50 [5, 79, 80, 81, 82]. The problem is even more complicated since the J/Ψ meson is not created instantly as a hadronic state and there is also a substantial ($\approx 35\%$) feeding from the $\chi_c - \gamma$ decays. Moreover, it is expected that the $c\bar{c}$ pair is first produced in a color-octet state together with a gluon (‘pre-resonance state’) and that this more extended configuration has a larger interaction cross section with baryons and mesons before the J/Ψ singlet state, Ψ' or χ_c finally emerges after some formation time τ_c . Additionally, the dissociation on mesons of formed J/Ψ 's will differ from χ_c due to their different thresholds with respect to the $D\bar{D}$ channel as well as for the Ψ' . Since experimental information on the various charmonium-meson cross sections – especially at low relative momenta – will be hard to obtain, the excitation function of charmonium suppression in central nucleus-nucleus collisions might be exploited to obtain additional information on the absorption scenarios. One expects that quite below the bombarding energy necessary for the formation of a QGP phase the charmonium absorption should be entirely due to dissociation with hadrons; any additional suppression due to color screening then will show up in a more rapid suppression with the incident energy or with the energy density achieved [83].

In this Section we calculate the excitation function for J/Ψ suppression within two absorption scenarios, i.e. the ‘early’ and ‘late’ comover dissociation models, which have been explored in detail by our group before at SPS energies [84, 85, 86]. The ‘early’ comover absorption scenario is based on the idea, that a $c\bar{c}$ pair is created in the initial ‘hard’ phase of the nucleus-nucleus collision, where the string density is very high, and the $c\bar{c}$ pair is dissolved in the color electric field of neighboring strings. Since in the HSD approach the information on the string density as well as the string space-time extension is available, the absorption model has only a single parameter, i.e. the average transverse dimension of an extending string. In Ref. [86] a string radius of 0.2 fm was found to describe simultaneously the data for p + A and S + U at 200 A·GeV from NA38 [62] and for Pb + Pb at 160 A·GeV

from NA50 [63] when adopting the conventional charmonium-nucleon dissociation cross section of 6 mb. It has been also speculated that the overlap of strings due to percolation might describe the phase transition to a QGP [87].

In the 'late' comover scenario the additional charmonium suppression is due to charmonium-meson scattering to $D\bar{D}$ with an average charmonium-meson cross section of ≈ 3 mb [85]. Cross sections of this order have been calculated by Haglin in Ref. [79] within a meson-exchange model and thus might appear not unrealistic. In our present calculation we refer to the model II of Ref. [85] including a 'pre-resonance' charmonium life time of 0.3–0.5 fm/c which is supported (within the errorbars) by a more recent analysis of charmonium suppression as a function of the Feynman variable x_F in p + A reactions [88] from He et al. [89] and Kharzeev et al. [90]. We recall that within the model II of Ref. [85] the J/Ψ suppression data for p + A and S + U at 200 A·GeV from NA38 [62] and for Pb + Pb at 160 A·GeV from NA50 [63] have been described very well when adopting a 'pre-resonance'-nucleon cross section of 6 mb and a J/Ψ -nucleon cross section of 3–4 mb in line with the data on J/Ψ photoproduction [91]. Independent dynamical studies on charmonium suppression within the UrQMD model [92, 93] later on have lead to very similar conclusions.

Since the comparison of our calculations at SPS energies has been performed to data taken in 1995 and before we show in Fig. 10 a comparison of the 'early' comover model (dashed line) [86] and the 'late' comover model II [85] with the more recent data from NA50 [76, 94] for Pb + Pb at 160 A·GeV using the explicit numbers from Refs. [85, 86]¹. The 'early' comover absorption model here gives a little too low suppression at high E_T whereas the 'late' comover absorption model is still in line with the more recent data from 1996 and 1998 with minimum bias (open triangles and open circles). The data from 1996 (full squares), that show a (much debated) two-step behaviour, do not agree with the explicit E_T dependence from our calculations; however, the 1996 minimum bias data (open triangles) well match for $E_T \geq 40$ GeV whereas the J/Ψ suppression is slightly overestimated at lower E_T . We do not comment on the highest E_T data points from 1998 with minimum bias since our earlier analysis did not extend to these specific events.

The question now arises, if the excitation function for J/Ψ suppression in central Au + Au collisions might show some unusual behaviour within the two scenarios discussed above or how they might be disentangled. In order to achieve the same suppression factor in central collisions within the 'early' comover model we have increased the string absorption radius from $r_s = 0.2$ fm to 0.22 fm to get the same value for the J/Ψ survival factor $S_{J/\Psi}$ at 160 A·GeV. We note that the total J/Ψ multiplicity shown in Fig. 5 has been calculated within the 'late' comover model. It drops by almost 3 orders of magnitude when decreasing the bombarding energy from 160 A·GeV to 20 A·GeV. At the lowest energy considered here the experimental J/Ψ signal will be very hard to measure; it is hopeless within the present experimental setups. Nevertheless, it is worth exploring theoretically if some unusual excitation function might be found. Our results are displayed in Fig. 11 (l.h.s.) for the 'early' absorption model (open circles) and for the 'late' comover model (full circles); both models practically do not differ in their excitation functions and show a very smooth decrease of $S_{J/\Psi}$ from 0.4 to 0.3 with increasing bombarding energy. The net absorption by baryons is dominant in both scenarios, however, differs in magnitude due to the simple fact that in the

¹This comparison is necessary since the 1995 data have been rescaled in [94] and our calculations are reported inconsistently in the more recent presentations of this topic [94, 95].

'early' (string) absorption model there is less suppression by baryons since the absorption by strings competes at early times. In the 'late' comover model there is more absorption by baryons because the mesons are formed at later stages and not competitive in the early phase; their relative contribution is lower as for strings accordingly. However, these individual contributions cannot be distinguished experimentally and thus are 'irrelevant'.

The r.h.s. of Fig. 11 shows the survival probability $S_{J/\Psi}$ in the 'late' comover model for central Au + Au collisions from 0.160 A·TeV to 21.5 A·TeV, respectively, where we have gated on J/Ψ 's in the rapidity interval $-1 \leq y_{cm} \leq 1$. The solid line stands for the total J/Ψ survival probability while the dashed line displays the relative absorption on baryons and the dotted line the relative dissociation on mesons. Whereas the dissociation on baryons is practically constant with bombarding energy, the absorption on mesons increases in line with the higher meson densities achieved with increasing E/A . We note that the 'early' comover model leads to a similar total absorption within the numerical accuracy.

We have to mention that neither the 'early' nor the 'late' comover model might be realized in nature exclusively and both absorption processes should occur within the same reaction with probably different weights. Since we do not find a substantial difference for both scenarios also a linear combination of both absorption models, i.e. decreasing r_s as well as the charmonium-meson cross section accordingly, will lead to a similar excitation function. This also holds for the relative suppression on the transverse energy E_T (cf. Fig. 10).

Inspite of the rather disappointing perspectives to disentangle the 'late' and 'early' comover models experimentally at the full range of SPS energies, the excitation function of J/Ψ still might show some discontinuity in E/A experimentally, which could rule out the two models studied here and indicate a transition to a QGP phase. This subject is taken up in the next Section again with respect to the dependence of $S_{J/\Psi}$ on the transverse energy E_T produced in Au + Au collisions at RHIC energies.

6 Predictions for RHIC energies

As noted in the introduction one expects that the initial nonequilibrium phase of a nucleus-nucleus collision at RHIC energies should be described by parton degrees of freedom, whereas hadrons are only formed (by 'condensation') at a later stage of the reaction and interact until freeze out. Thus parton cascade calculations should be adequate for all initial reactions involving a large 4-momentum transfer between the constituents, while hadron cascades should be appropriate in the final hadronic expansion phase. We suggest that the dynamics in between the partonic and hadronic phase might be described by quarks (diquarks) and strings as e.g. implemented in the HSD approach.

The practical question is, however, if nonequilibrium partonic and hadron/string models can be distinguished at all, i.e. do they lead to different predictions for experimental observables? In fact, first applications of the parton cascade model developed by Geiger [8, 96] to nucleus-nucleus collisions at SPS energies [97] have suggested that a reasonable description of the meson and baryon rapidity distributions can also be achieved on the basis of partonic degrees of freedom. However, in the latter calculations the extrapolation of the strong coupling constant to low Q^2 has been overestimated as discovered recently by Bass

and Müller [98]. This finding invalidates the detailed predictions and comparisons within the hybrid models VNI+UrQMD or VNI+HSD presented in Ref. [99] that have been tailored to describe the dynamics at RHIC or even LHC energies.

We start with pp collisions at $\sqrt{s} = 200$ GeV. The calculated results for the proton, π^+ and K^+ rapidity distributions in the cms are shown in Fig. 12 (upper part) for both models, which are denoted individually by the labels VNI and HSD in obvious notation. On the level of pp collisions we find only minor differences between the two kinetic models. The parton cascade shows a slightly higher amount of proton stopping as the HSD model (l.h.s.) and as a consequence a slightly higher production of π^+ and K^+ mesons (r.h.s.), because the energy taken from the relative motion of the leading baryons is converted to the production of mesons. It is presently unclear which of the two approaches will be closer to experiment; a proper description of pp data will be a necessary step before performing reliable extrapolations to nucleus-nucleus collisions.

In spite of this missing experimental information we directly step towards central collisions ($b \leq 1.5$ fm) for Au + Au at $\sqrt{s} = 200$ GeV. The calculated results for the net proton (here $p - \bar{p}$), antiproton, π^+ and K^+ rapidity distributions in the cms are shown in Fig. 12 (lower part). In the HSD scenario essentially 'comover' scattering occurs with a low change of the meson rapidity distribution. Thus the meson rapidity distributions are roughly the same as for pp collisions. Also note that at midrapidity the net baryon density $\sim N_p - N_{\bar{p}}$ is practically zero, however, even at midrapidity a lot of baryons appear that are produced together with antibaryons. Thus also mesons (especially $c\bar{c}$ pairs) encounter a lot of baryons and antibaryons on their way to the continuum. Whereas the HSD approach predicts a vanishing net baryon density at midrapidity, other recent models – that combine high and low energy transport concepts – suggest a sizeable net proton density for $y_{cm} \approx 0$ [100].

The amount of higher order hadronic rescattering processes at RHIC energies is depicted in Fig. 13 (lower right part) as emerging from the HSD calculation, where the number of baryon-baryon (BB) and meson-baryon collisions (mB) is shown as a function of the invariant energy \sqrt{s} . We mention that quark-baryon and diquark-baryon collisions are counted here as mB or BB collisions, respectively. Apart from the initial small peak at $\sqrt{s} = 200$ GeV a substantial amount of intermediate and low energy rescattering processes with maxima at 2.5 GeV and 1.8 GeV are found, which essentially stand for flavor exchange processes, multiple pion production in mB and BB collisions as well as secondary strangeness production channels. For comparison the corresponding \sqrt{s} distributions are also displayed for bombarding energies of 2, 11 and 160 A·GeV, respectively, showing a dominance of low energy BB and mB collisions. The latter reactions occur at energy scales where perturbative QCD is no longer applicable. This has to be kept in mind additionally when comparing to pp and pA reactions at $\sqrt{s} = 200$ GeV.

We return to the question of charmonium suppression at RHIC energies since it is expected that one might probe increasing energy densities also with increasing centrality of the collision, where the latter can be correlated with the transverse energy E_T produced in a collision event. As argued e.g. by Satz [83] the survival factor $S_{J/\Psi}$ then should show steps as a function of E_T due to the melting of first the χ_c and then the J/Ψ in a QGP phase. As seen from Fig. 10 there are no pronounced steps in the E_T dependence of J/Ψ suppression in the data for Pb + Pb at SPS energies according to the authors point of view; this situation might change at RHIC energies.

Using the 'late' comover model described in Section 5 we have calculated the J/Ψ survival factor $S_{J/\Psi}$ as a function of the transverse energy E_T in the cms rapidity window $[-1,1]$ for Au + Au at $\sqrt{s} = 200$ GeV on an event by event basis covering all impact parameters from $b = 0$ to 13 fm. The resulting correlation of $S_{J/\Psi}$ with E_T is shown in Fig. 14 and indicates a smooth decrease with centrality (or increasing E_T) reaching an average survival probability of ≈ 0.1 for the most central events (cf. Fig. 11, r.h.s.). This result can be understood as follows: According to our calculations the net J/Ψ dissociation by mesons in central Au + Au collisions at the SPS is $\approx 16\%$ (cf. Fig. 11) while the rapidity distribution of negatively charged particles (h^-) at midrapidity here is about 180. At the RHIC energy we get a corresponding h^- rapidity density at midrapidity of ≈ 450 (cf. Fig. 12) which is higher by a factor of 2.5. Simply multiplying the J/Ψ meson absorption at the SPS of 16% by the factor 2.5 we obtain about 40% for central collisions at RHIC energies, which together with $\approx 52\%$ of absorption on baryons gives a survival probability of 8%. The actual numerical results in Fig. 14 indicate that this simple estimate works quite well. On the other hand, if the h^- rapidity density is found to be lower (higher) experimentally, we expect corresponding changes in the J/Ψ suppression for central events if the 'late' comover absorption model holds true. This dependence might well be tested experimentally in the near future to possibly falsify the comover dissociation model.

7 Summary

In this work we have performed a systematic analysis of hadron production in central Au + Au collisions from SIS to RHIC energies within the HSD transport approach. We have concentrated here on the 'classical' signatures, i.e. strangeness and low mass dilepton enhancement as well as charmonium suppression. For all observables our calculations give a monotonic increase (for the ratio K^+/π^+ and charmonium suppression) or decrease (for the low mass dilepton enhancement) with bombarding energy, respectively. So far, experimental data are available only in a limited range of bombarding energies or at a single energy, respectively. We have pointed out that the relative maximum indicated by the experimental data in the K^+/π^+ ratio at about 10 A·GeV (or higher?) is not reproduced within the transport approach that is based on quark, diquark, string and hadronic degrees of freedom. We speculate that at AGS energies this failure might be attributed to a restoration of chiral symmetry in a sufficiently large space-time volume (cf. Figs. 3 and 4).

The enhancement of low mass dileptons in the range $0.3 \text{ GeV} \leq M_{e^+e^-} \leq 0.6 \text{ GeV}$ is most pronounced at lower bombarding energies of 2–5 A·GeV within our calculations since here the space-time volume for densities above $2 \rho_0$ is very large such that a majority of ρ -mesons probes the high density phase of the reaction (cf. Fig. 5). With increasing bombarding energy the average density – which a ρ -meson experiences – drops substantially such that high energy nucleus-nucleus collisions are not well suited for in-medium ρ spectroscopy.

The suppression of charmonium (here J/Ψ) increases smoothly with bombarding energy and centrality of the reaction within the 'early' and 'late' comover absorption scenarios. Unfortunately, both scenarios cannot be distinguished by means of the excitation function since they give approximately the same survival probability $S_{J/\Psi}$ with bombarding energy (cf. Fig. 11). In the transport approach the smooth increase of charmonium absorption with

bombarding energy is easy to understand: a major fraction of J/Ψ 's is anyhow dissociated by baryons which basically are of the same number at all energies considered here; only the relative collisional energy changes. The additional absorption by 'early' strings or 'late' hadrons increases smoothly with bombarding energy since the string and hadron density increases accordingly. At RHIC energies this additional suppression mechanism leads to a J/Ψ suppression of about 90% in central Au + Au collisions even without employing an explicit formation of a QGP. We note, however, that the charmonium suppression shows a smooth dependence on the transverse energy E_T (cf. Fig. 14); any gradual steps of $S_{J/\Psi}$ with E_T due to a melting of the χ_c or the J/Ψ at higher energy density would indicate a new suppression mechanism which might be attributed to color screening in a QGP phase [83].

The authors acknowledge inspiring discussions with J. Aichelin, S. A. Bass, G. E. Brown, C. Greiner, M. Gyulassy, C. M. Ko, U. Mosel, R. Rapp, H. Satz, H. Sorge, H. Stöcker, J. Wambach, X.-N. Wang and K. Werner.

References

- [1] J. W. Harris and B. Müller, *Annu. Rev. Nucl. Part. Sci.* 46 (1996) 71.
- [2] E. V. Shuryak, *Rev. Mod. Phys.* 65 (1993) 1.
- [3] Quark Matter'99, *Nucl. Phys. A* (1999) , in press.
- [4] K. Geiger and B. Müller, *Nucl. Phys. B* 369 (1992) 600.
- [5] B. Müller, *nucl-th/9906029*, *Nucl. Phys. A*, in press.
- [6] H. Sorge, *nucl-th/9906051*, *Nucl. Phys. A*, in press.
- [7] S. A. Bass et al., *Prog. Part. Nucl. Phys.* 41 (1998) 225; *J. Phys. G* 25 (1999) R1.
- [8] K. Geiger, *Phys. Rep.* 258 (1995) 237.
- [9] X.-N. Wang, *Phys. Rep.* 280 (1997) 287.
- [10] W. Cassing and E. L. Bratkovskaya, *Phys. Rep.* 308 (1999) 65.
- [11] W. Ehehalt and W. Cassing, *Nucl. Phys. A* 602 (1996) 449.
- [12] J. Geiss, W. Cassing, and C. Greiner, *Nucl. Phys. A* 644 (1998) 107.
- [13] G. E. Brown and M. Rho, *Phys. Rev. Lett.* 66 (1991) 2720.
- [14] V. Koch, *Int. J. Mod. Phys. E* 6 (1997) 203.
- [15] J. V. Steele, H. Yamagishi, and I. Zahed, *Phys. Lett. B* 384 (1996) 255; *Phys. Rev. D* 56 (1997) 5605.

- [16] H. Stöcker and W. Greiner, Phys. Rep. 137 (1986) 277.
- [17] G. F. Bertsch and S. Das Gupta, Phys. Rep. 160 (1988) 189.
- [18] W. Cassing, V. Metag, U. Mosel, and K. Niita, Phys. Rep. 188 (1990) 363.
- [19] C. M. Ko and G. Q. Li, J. Phys. G 22 (1996) 1673.
- [20] W. Botermans and R. Malfliet, Phys. Rep. 198 (1990) 115.
- [21] R. Malfliet, Prog. Part. Nucl. Phys. 21 (1988) 207.
- [22] A. Faessler, Prog. Part. Nucl. Phys. 30 (1993) 229.
- [23] G. E. Brown, Prog. Theor. Phys. 91 (1987) 85.
- [24] G. E. Brown, C. M. Ko, Z. G. Wu, and L. H. Xia, Phys. Rev. C 43 (1991) 1881.
- [25] V. Koch and G. E. Brown, Nucl. Phys. A 560 (1993) 345.
- [26] B. Peterson, Nucl. Phys. B 30 (1992) 66.
- [27] F. Karsch, Nucl. Phys. B 34 (1993) 63.
- [28] J. Engels, Phys. Lett. B 252 (1990) 625; J. Engels, F. Karsch and K. Redlich, Nucl. Phys. B 435 (1995) 295.
- [29] F. Karsch and E. Laermann, Phys. Rev. D 50 (1994) 6954.
- [30] W. Cassing and U. Mosel, Prog. Part. Nucl. Phys. 25 (1990) 235.
- [31] K. Weber, B. Blättel, W. Cassing, H.-C. Dönges, V. Koch, A. Lang, and U. Mosel, Nucl. Phys. A 539 (1992) 713.
- [32] S. Hama, B. C. Clark, E. D. Cooper, H. S. Sherif and R. L. Mercer, Phys. Rev. C 41 (1990) 2737.
- [33] B. Nilsson-Almqvist and E. Stenlund, Comp. Phys. Comm. 43 (1987) 387; B. Anderson, G. Gustafson and Hong Pi, Z. Phys. C 57 (1993) 485.
- [34] J. Schwinger, Phys. Rev. 83 (1951) 664
- [35] H.-U. Bengtsson and T. Sjöstrand, Computer Physics Commun. 46 (1987) 43.
- [36] E. G. Drukarev and E. M. Levin, Nucl. Phys. A 511 (1990) 679.
- [37] B. Friman, W. Nörenberg and V. D. Toneev, Eur. Phys. J. A 3 (1998) 165.
- [38] E. L. Bratkovskaya and W. Cassing, Nucl. Phys. A 619 (1997) 413.
- [39] P. K. Sahu, W. Cassing, U. Mosel, and A. Ohnishi, nucl-th/9907002.
- [40] E. L. Bratkovskaya, W. Cassing, C. Greiner et al., preprint UGI-99-32.

- [41] W. Cassing, E. L. Bratkovskaya, U. Mosel, S. Teis, and A. Sibirtsev, Nucl. Phys. A 614 (1997) 415.
- [42] E. L. Bratkovskaya, W. Cassing and U. Mosel, Nucl. Phys. A 622 (1997) 593.
- [43] E. L. Bratkovskaya, W. Cassing and U. Mosel, Phys. Lett. B 424 (1998) 244.
- [44] E. L. Bratkovskaya, W. Cassing, R. Rapp, and J. Wambach, Nucl. Phys. A 634 (1998) 168.
- [45] *Strangeness in Quark Matter 1998*, J. Phys. G 25 (1999) 143.
- [46] C. A. Ogilvie for the E866 and E819 Collaboration, Nucl. Phys. A 638 (1998) 57c; J. Phys. G 25 (1999) 159.
- [47] L. Ahle et al., Nucl. Phys. A 610 (1996) 139c; Phys. Rev. C 57 (1998) R466; Phys. Rev. C 60 (1999) 044904.
- [48] P. Braun-Munzinger, J. Stachel, J. P. Wessels, and N. Xu, Phys. Lett. B 344 (1995) 43; Phys. Lett. B 365 (1996) 1.
- [49] F. Wang, H. Liu, H. Sorge, N. Xu, and J. Yang, nucl-th/9909001.
- [50] H. Sorge, Z. Phys. C 67 (1995) 479; Phys. Rev. C 52 (1995) 3291; Nucl. Phys. A 630 (1998) 522c.
- [51] E. Shuryak, Phys. Lett. B 78 (1978) 150; Sov. J. Nucl. Phys. 28 (1978) 408.
- [52] K. Kajantie, J. Kapusta, L. McLerran, and A. Mekjian, Phys. Rev. D 34 (1986) 2746.
- [53] P. V. Ruuskanen, Nucl. Phys. A 544 (1992) 169c.
- [54] J. Cleymans, K. Redlich and H. Satz, Z. Phys. C 52 (1991) 517.
- [55] U. Heinz and K. S. Lee, Phys. Lett. B 259 (1991) 162.
- [56] F. Klingl, N. Kaiser and W. Weise, Nucl. Phys. A 624 (1997) 527.
- [57] G. Roche et al., Phys. Rev. Lett. 61 (1988) 1069; C. Naudet et al., Phys. Rev. Lett. 62 (1989) 2652; G. Roche et al., Phys. Lett. B 226 (1989) 228.
- [58] G. Agakichiev et al., Phys. Rev. Lett. 75 (1995) 1272.
- [59] G. Agakichiev et al., Phys. Lett. B 422 (1998) 405.
- [60] M. A. Mazzoni, Nucl. Phys. A 566 (1994) 95c; M. Masera, Nucl. Phys. A 590 (1995) 93c.
- [61] T. Åkesson et al., Z. Phys. C 68 (1995) 47.
- [62] C. Baglin et al., Phys. Lett. B 220 (1989) 471; B 251 (1990) 465; B 270 (1991) 105; B 345 (1995) 617; S. Ramos, Nucl. Phys. A 590 (1995) 117c.

- [63] M. Gonin et al., Nucl. Phys. A 610 (1996) 404c.
- [64] C. M. Ko, V. Koch and G. Q. Li, Ann. Rev. Nucl. Part. Sci. 47 (1997) 505.
- [65] R. Rapp, G. Chanfray and J. Wambach, Phys. Rev. Lett. 76 (1996) 368.
- [66] B. Friman and H. J. Pirner, Nucl. Phys. A 617 (1997) 496.
- [67] R. Rapp, G. Chanfray and J. Wambach, Nucl. Phys. A 617 (1997) 472.
- [68] R. Rapp and J. Wambach, nucl-th/9909229, to appear in Adv. Nucl. Phys.
- [69] E. L. Bratkovskaya and C. M. Ko, Phys. Lett. B 445 (1999) 265.
- [70] W. K. Wilson et al., Phys. Rev. C 57 (1998) 1865.
- [71] E. L. Bratkovskaya, W. Cassing, M. Effenberger, and U. Mosel, Nucl. Phys. A 653 (1999) 301.
- [72] C. Ernst, S. A. Bass, M. Belkacem et al., Phys. Rev. C 58 (1998) 447.
- [73] W. Cassing, E. L. Bratkovskaya, R. Rapp, and J. Wambach, Phys. Rev. C 57 (1998) 916.
- [74] T. Matsui and H. Satz, Phys. Lett. B 178 (1986) 416.
- [75] M. Gonin et al., Nucl. Phys. A 610 (1996) 404c.
- [76] M. C. Abreu et al., Phys. Lett. B 450 (1999) 456.
- [77] R. Vogt, Phys. Rep. 310 (1999) 197.
- [78] X.-N. Wang and B. Jacak, Eds., *Quarkonium production in high-energy nuclear collisions*, World-Scientific, 1998.
- [79] K. Haglin, nucl-th/9907034.
- [80] S. G. Matinyan and B. Müller, Phys. Rev. C 58 (1998) 2994.
- [81] K. Martins, D. Blaschke and E. Quack, Phys. Rev. C 51 (1995) 2723.
- [82] D. Kharzeev and H. Satz, Phys. Lett. B 334 (1994) 155.
- [83] H. Satz, Quark Matter'99, hep-ph/9908339, Nucl. Phys. A, in press.
- [84] W. Cassing and C. M. Ko, Phys. Lett. B 396 (1997) 39.
- [85] W. Cassing and E. L. Bratkovskaya, Nucl. Phys. A 623 (1997) 570.
- [86] J. Geiss, C. Greiner, E.L. Bratkovskaya, W. Cassing, and U. Mosel, Phys. Lett. B 447 (1999) 31.

- [87] H. Satz, Nucl. Phys. A 642 (1998) 130; M. Nardi and H. Satz, Phys. Lett. B 442 (1998) 14.
- [88] M. J. Leitch, E866 Collaboration, Quark Matter'99, Nucl. Phys. A, in press.
- [89] Y. B. He, J. Hüfner and B. Z. Kopeliovich, hep-ph/9908243.
- [90] D. Kharzeev and R. L. Thews, Phys. Rev. C 60 (1999) 041901.
- [91] U. Camerini et al., Phys. Rev. Lett. 35 (1975) 483; B. Gittelman et al., Phys. Rev. Lett. 35 (1975) 1616; S. Aid et al., Nucl. Phys. B 472 (1996) 3.
- [92] L. Gerland et al., Phys. Rev. Lett. 81 (1998) 762.
- [93] C. Spieles et al., Eur. Phys. J. C 5 (1998) 349; Phys. Rev. C 60 (1999) 054901.
- [94] C. Ciolo for the NA50 Collaboration, Quark Matter'99, Nucl. Phys. A, in press.
- [95] P. Braun-Munzinger, nucl-ex/9909014, Nucl. Phys. A, in press.
- [96] K. Geiger, Comp. Phys. Comm. 104 (1997) 70.
- [97] K. Geiger and D. K. Srivastava, Phys. Rev. C 56 (1997) 2718.
- [98] S. A. Bass and B. Müller, Preprint DUKE-TH-99-192.
- [99] S. A. Bass, M. Bleicher, W. Cassing et al., nucl-th/9907090, Nucl. Phys. A, in press.
- [100] B. Zhang, C. M. Ko, B. A. Li, and Z. Lin, nucl-th/9907017.

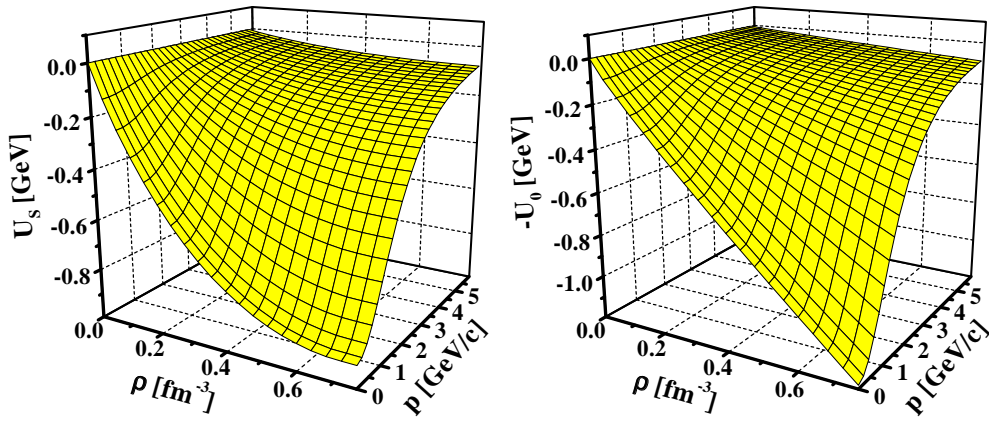


Figure 1: The nucleon scalar (U_S) and negative vector potential ($-U_0$) as a function of the nuclear density ρ and relative momentum p of the nucleon with respect to the nuclear matter rest frame as implemented in the HSD transport approach [11].

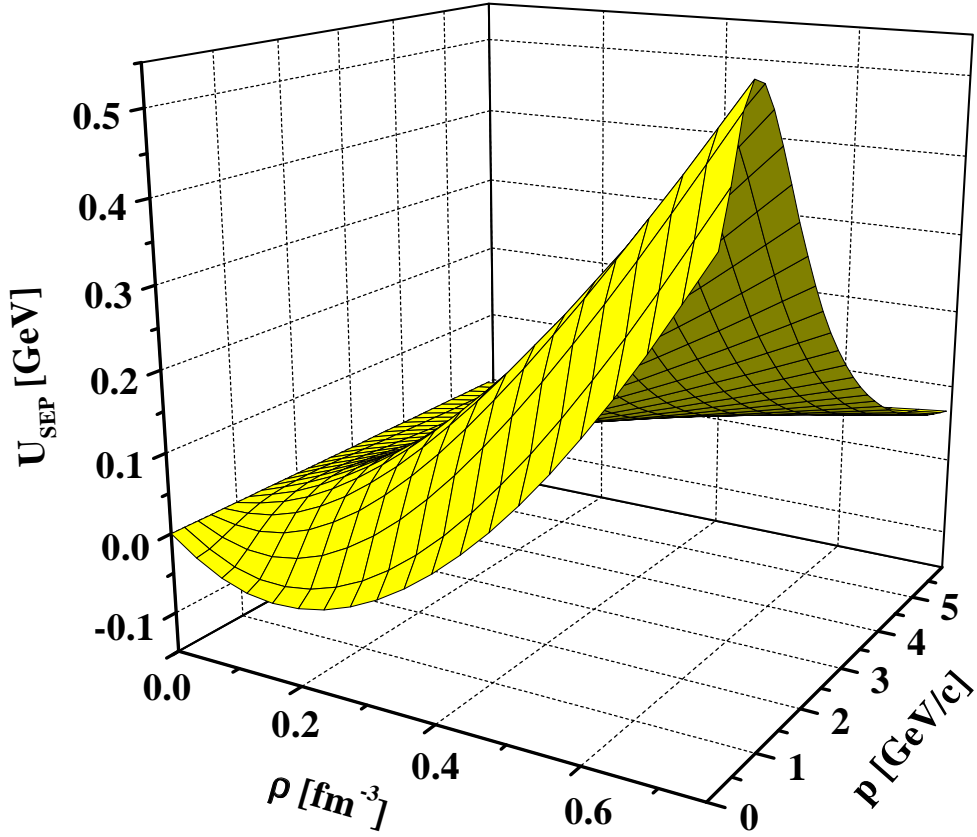


Figure 2: The potential U_{SEP} (5) – as resulting from the nucleon scalar (U_S) and vector potential (U_0) in Fig. 1 – as a function of the nuclear density ρ and relative momentum p of the nucleon with respect to the nuclear matter rest frame.

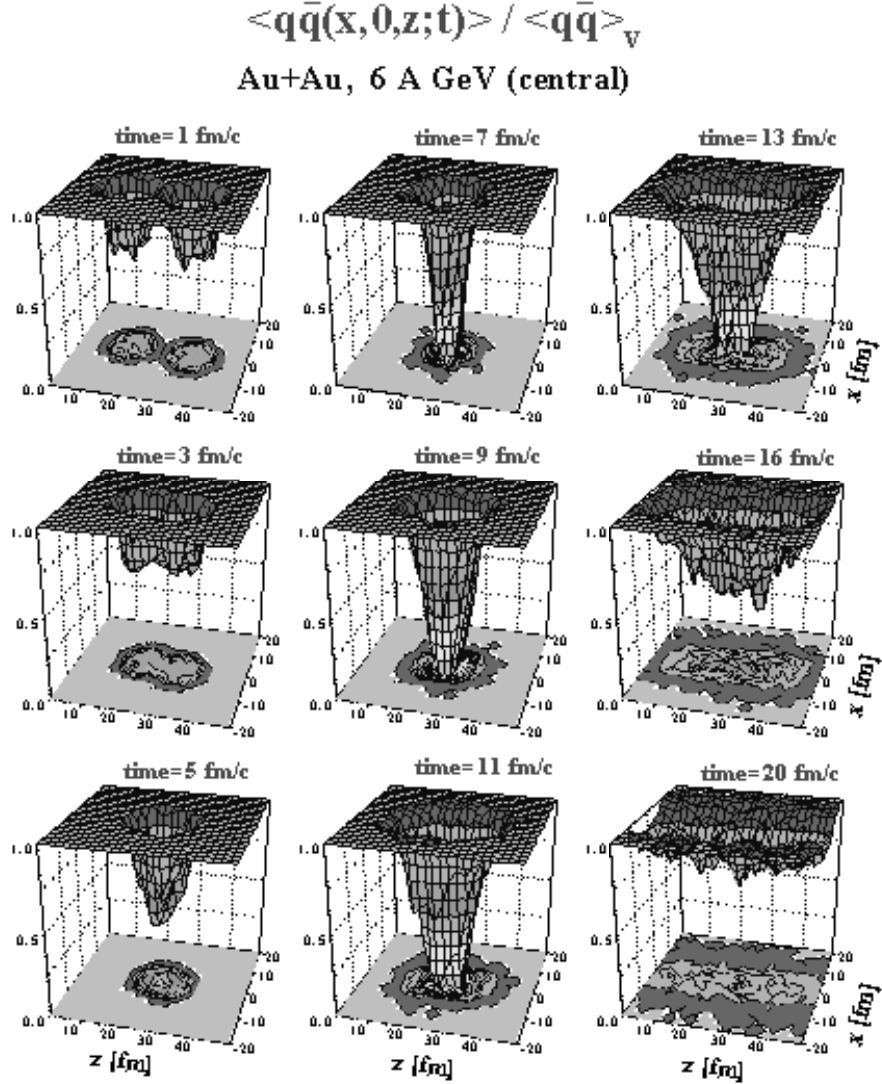


Figure 3: The scalar quark condensate $\langle q\bar{q}(x, 0, z; t) \rangle$ for central Au + Au collisions at 6 A-GeV divided by the vacuum condensate $\langle q\bar{q} \rangle_v$ such that the nonperturbative vacuum is characterized by a value of 1. The z -direction has been stretched by the Lorentz-factor γ_{cm} to compensate for Lorentz contraction, while negative numerical values for the condensate have been suppressed.

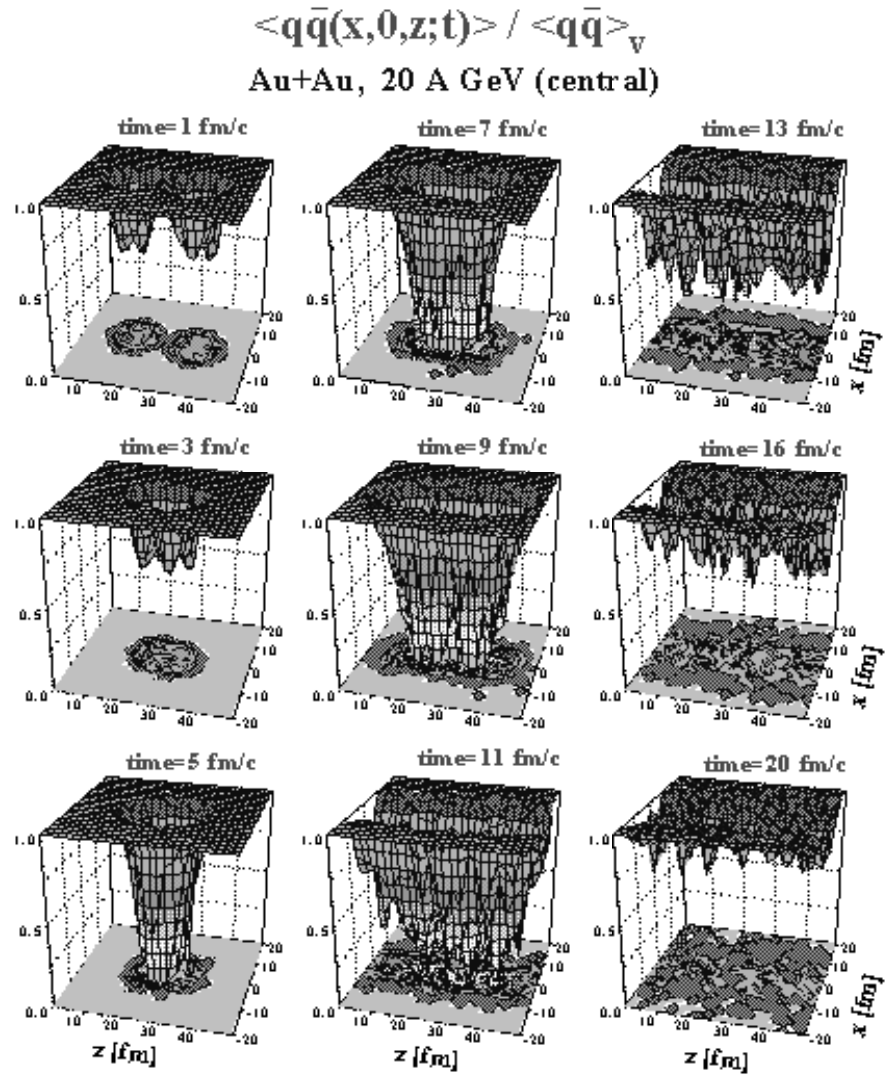


Figure 4: Same as Fig. 3 for central collisions of Au + Au at 20 A·GeV.

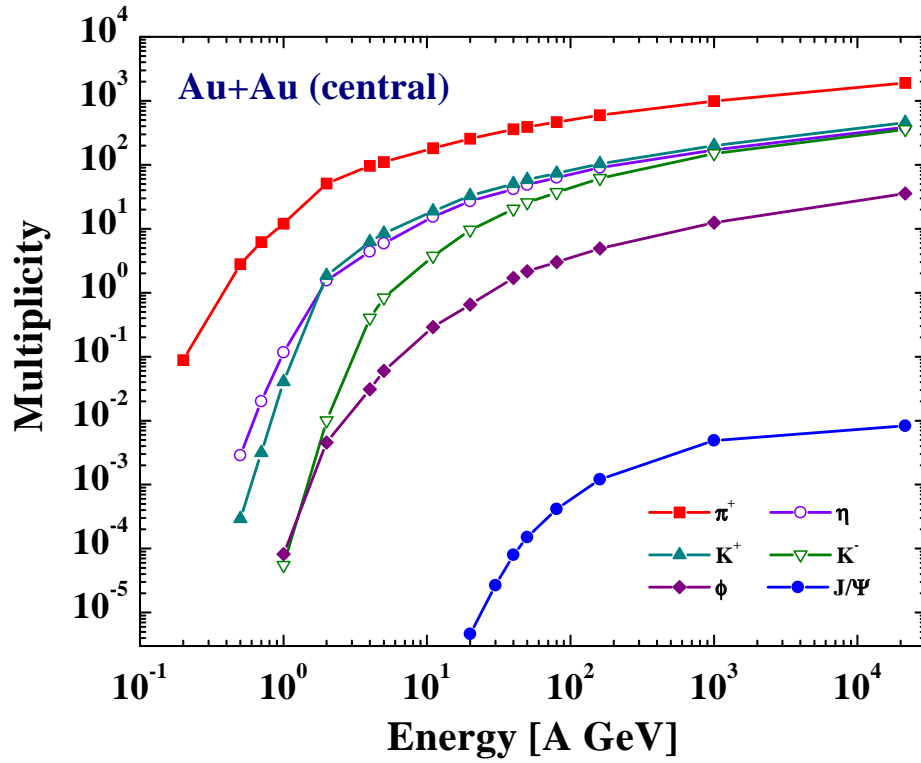


Figure 5: The meson (π^+ , η , K^+ , K^- , ϕ and J/Ψ) multiplicities from the HSD approach for central collisions of $Au + Au$ from 200 A MeV to 21.5 A·TeV.

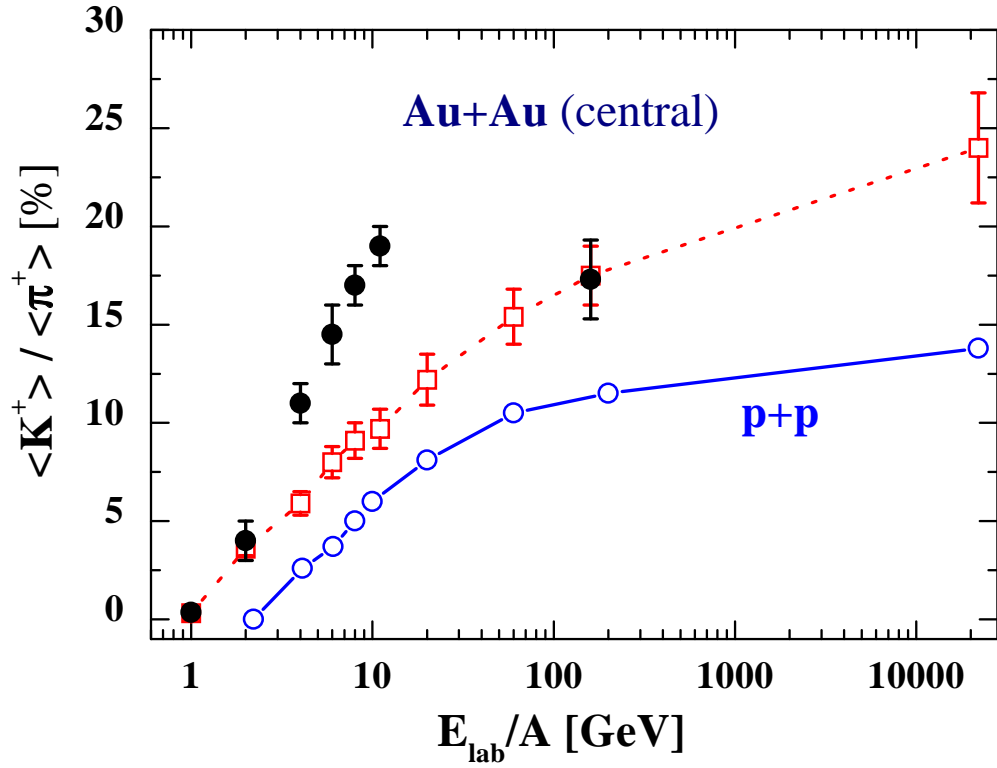


Figure 6: The K^+/π^+ ratio at midrapidity from central Au + Au ($Pb + Pb$) collisions from 1 A·GeV to 21.5 A·TeV. The open circles show the results from HSD for pp collisions while the open squares are obtained for central Au + Au reactions. The experimental data from Refs. [3, 46, 47] are displayed in terms of the full circles.

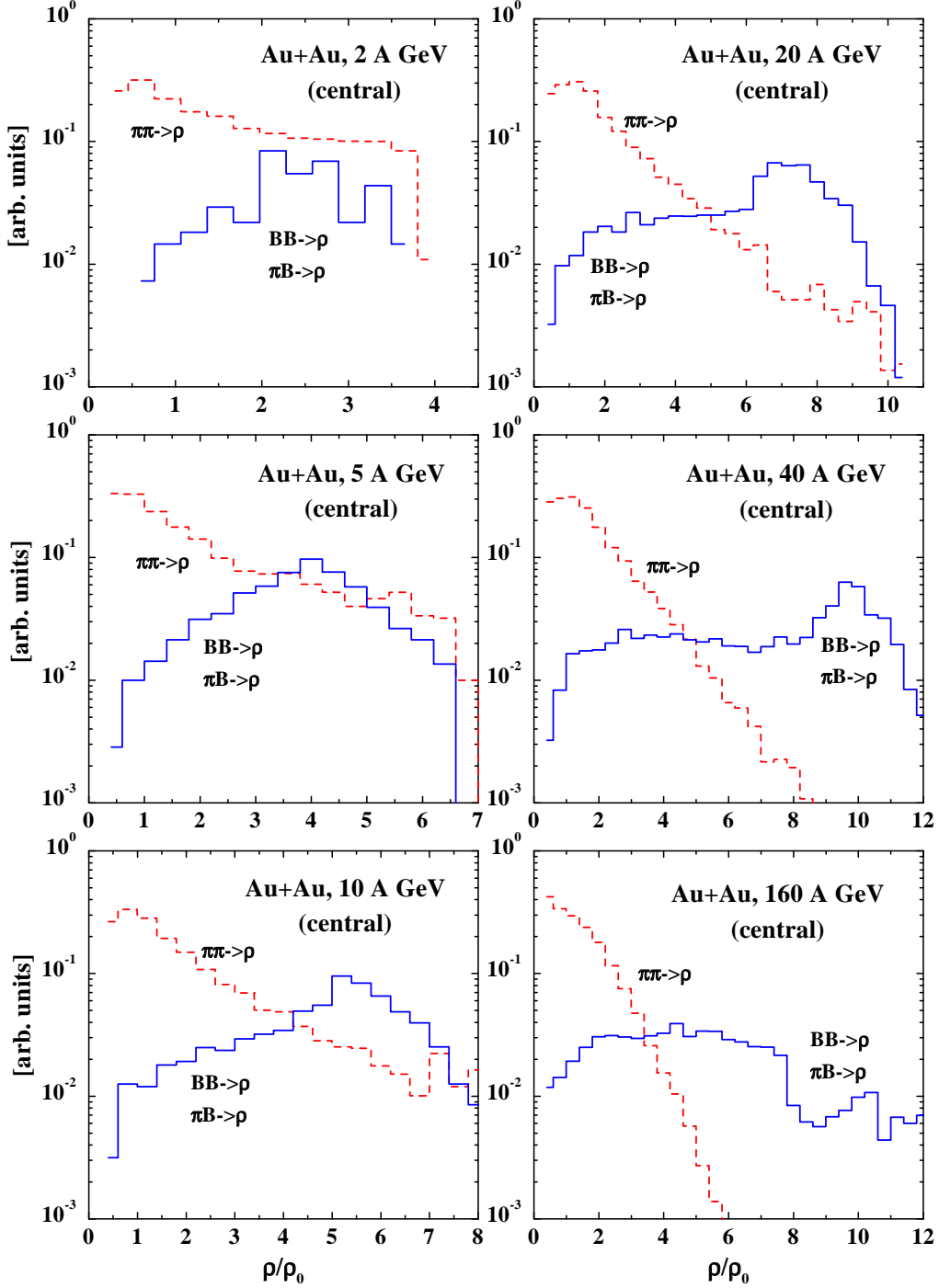


Figure 7: The differential ρ -meson distribution versus baryon density ρ/ρ_0 (at the ρ creation point) for central collisions of Au + Au at 2, 5, 10, 20, 40, and 160 A-GeV from the HSD approach. The production channels involving two baryons or a meson and a baryon (denoted by $BB \rightarrow \rho, \pi B \rightarrow \rho$) are summed up in the solid histograms whereas the dashed histograms stand for the sum of the meson production channels (denoted by $\pi\pi \rightarrow \rho$) which are dominated by the pion annihilation channel.

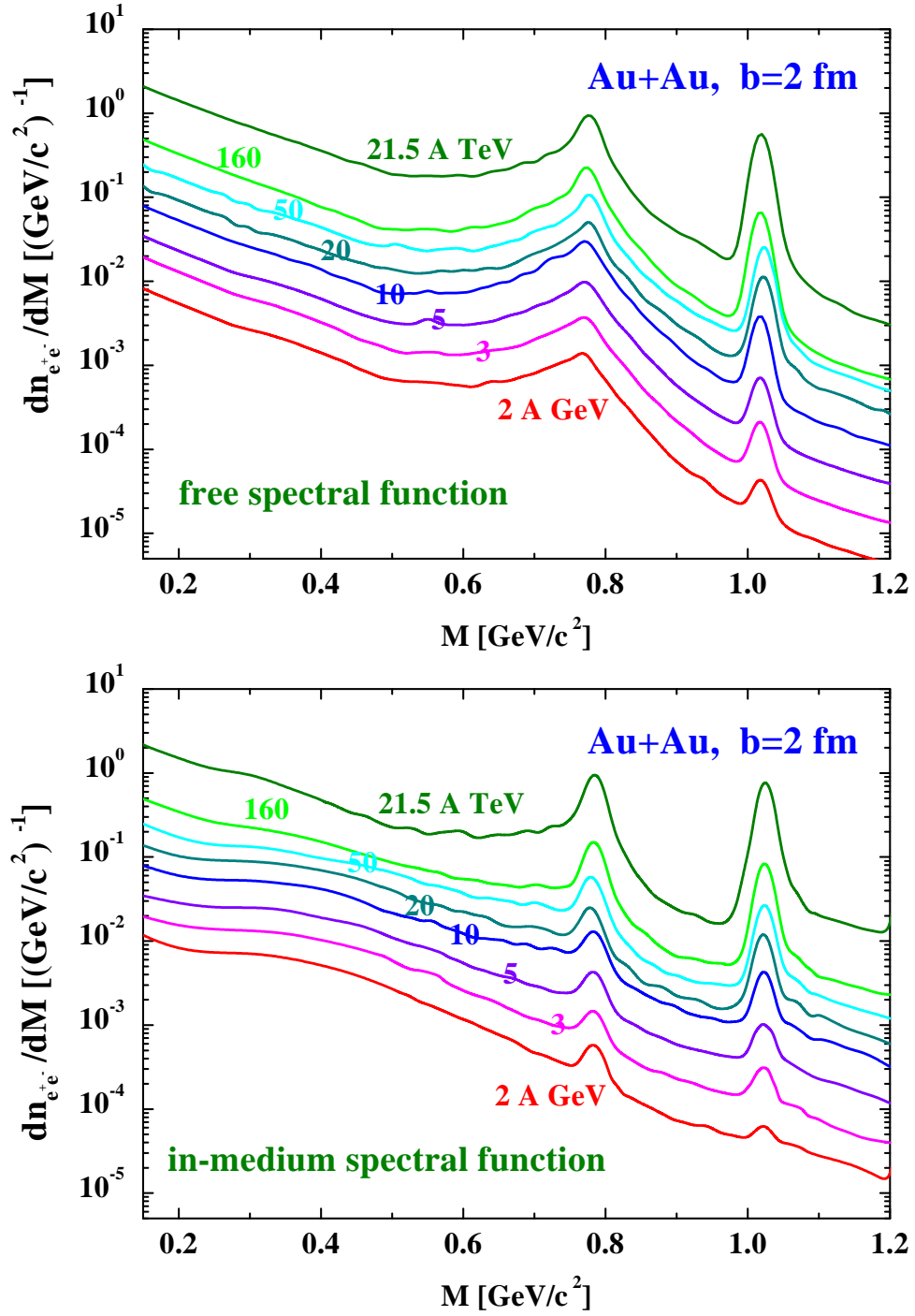


Figure 8: The differential dilepton multiplicity $dn_{e^+e^-}/dM$ for central collisions of Au + Au for 2, 3, 5, 10, 20, 50, 160, and 21500 A·GeV. Upper part: HSD calculations involving the 'free' ρ -meson spectral function: lower part: HSD calculation involving the in-medium ρ spectral function from Rapp et al. [67, 73].

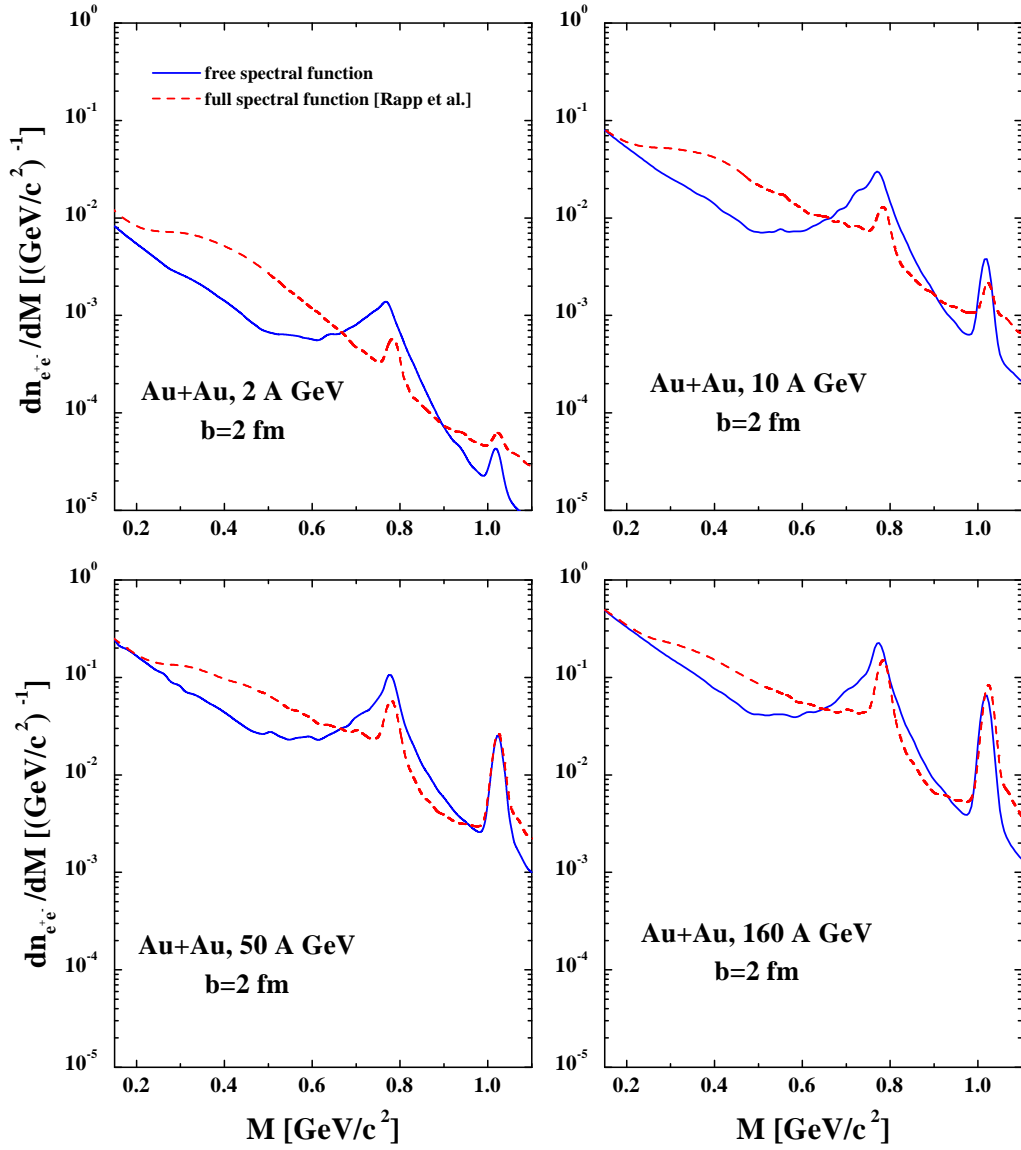


Figure 9: The differential dilepton multiplicity $dn_{e^+e^-}/dM$ for central collisions of Au + Au at 2, 10, 50, and 160 A·GeV from the HSD calculations involving the 'free' ρ -meson spectral function (solid lines) and the in-medium ρ spectral function from Rapp et al. [67, 73] (dashed lines) for comparison.

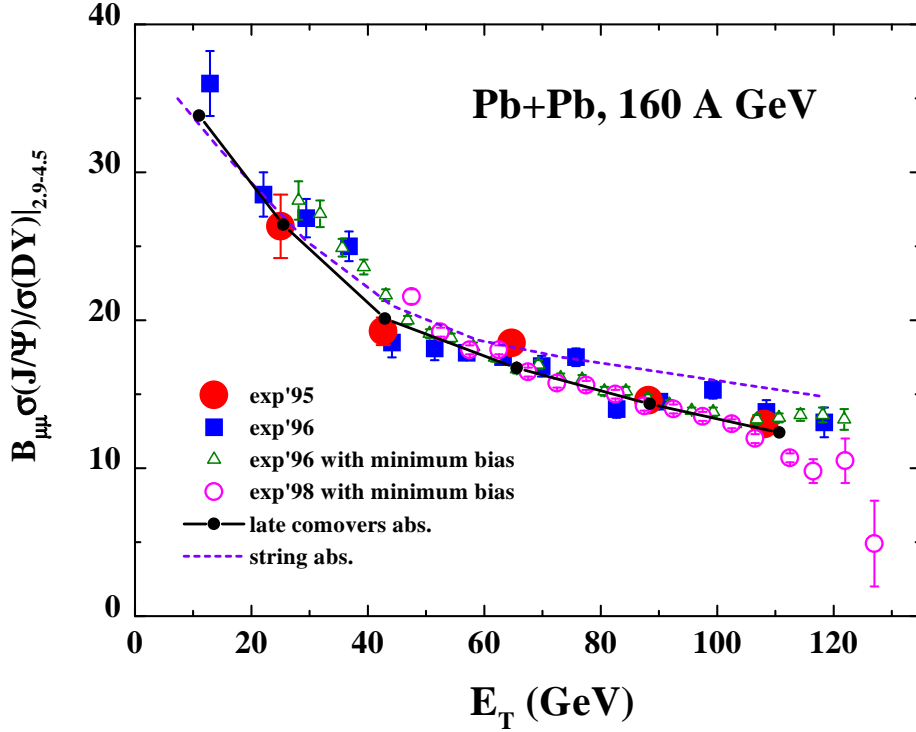


Figure 10: The J/Ψ suppression (in terms of the $\mu^+\mu^-$ decay branch relative to the Drell-Yan background from 2.9 – 4.5 GeV invariant mass) as a function of the transverse energy E_T in Pb + Pb collisions at 160 A·GeV. The solid line stands for the HSD result within the 'late' comover absorption scenario from Ref. [85] while the dashed line results from the 'early' string absorption scenario from Ref. [86] involving a transverse string radius $r_s = 0.2$ fm. The full dots stand for the NA50 data from 1995 [63], the full squares for the 1996 data [76], the open triangles for the 1996 data with minimum bias [76] while the open circles represent the 1998 data [94]. Note that the 1995 data have been rescaled in E_T as compared to Ref. [63]; the same rescaling has been adopted to the calculations from Refs. [85, 86] which had been compared to the data from [63].

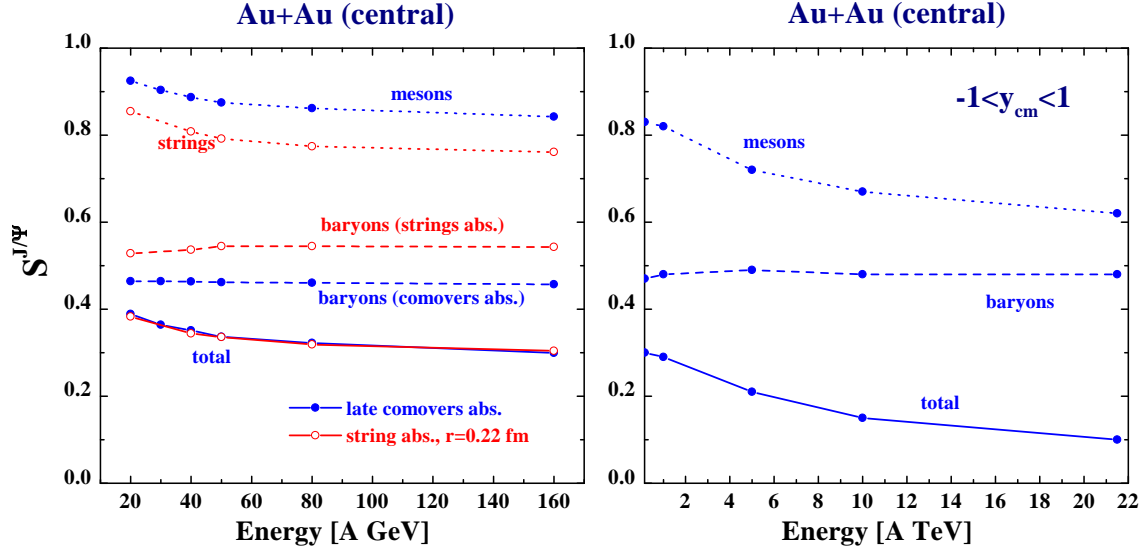


Figure 11: The J/Ψ survival factor $S^{J/\Psi}$ (in terms of the $\mu^+\mu^-$ decay branch relative to the Drell-Yan background from 2.9 – 4.5 GeV invariant mass normalized to the same quantity for pd reactions) as a function of the bombarding energy in central Au + Au collisions from 20 to 160 A·GeV (l.h.s.) and from 160 A·GeV to 21.5 A·TeV (r.h.s.). The solid line (full dots) stands for the HSD result within the 'late' comover absorption scenario from Ref. [85] while the solid line (open circles) results from the 'early' string absorption scenario from Ref. [86] involving a transverse string radius $r_s = 0.22$ fm in order to match both absorption scenarios at 160 A·GeV. The dashed lines stand for the relative fraction of J/Ψ dissociations with baryons while the dotted lines stand for the 'early' comover string dissociation (open circles) and 'late' comover meson dissociation (full dots), respectively. The total suppression factors (full lines) are practically identical for both scenarios from 20 to 160 A·GeV (l.h.s.). This also holds for the energy range from 160 A·GeV to 21.5 A·TeV within the numerical accuracy achieved.

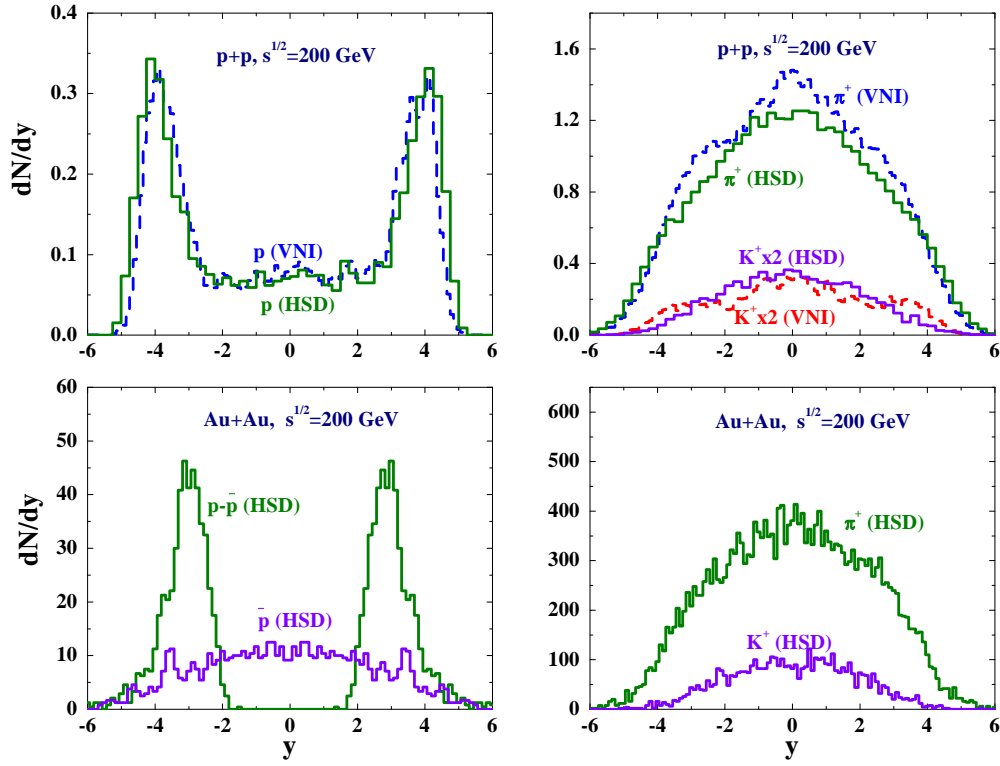


Figure 12: The rapidity distribution of protons (upper left part) from pp collisions at $\sqrt{s} = 200$ GeV from the HSD approach (solid histogram) in comparison to the prediction from the parton cascade VNI [96] (dashed histogram); the upper right part shows the same comparison for the π^+ and K^+ rapidity distributions, respectively. The lower part of the figure displays the HSD predictions for central ($b \leq 1.5$ fm) Au + Au at $\sqrt{s} = 200$ GeV per nucleon; (l.h.s.) net proton ($p - \bar{p}$) and \bar{p} rapidity distribution, (r.h.s.) π^+ and K^+ rapidity distributions.

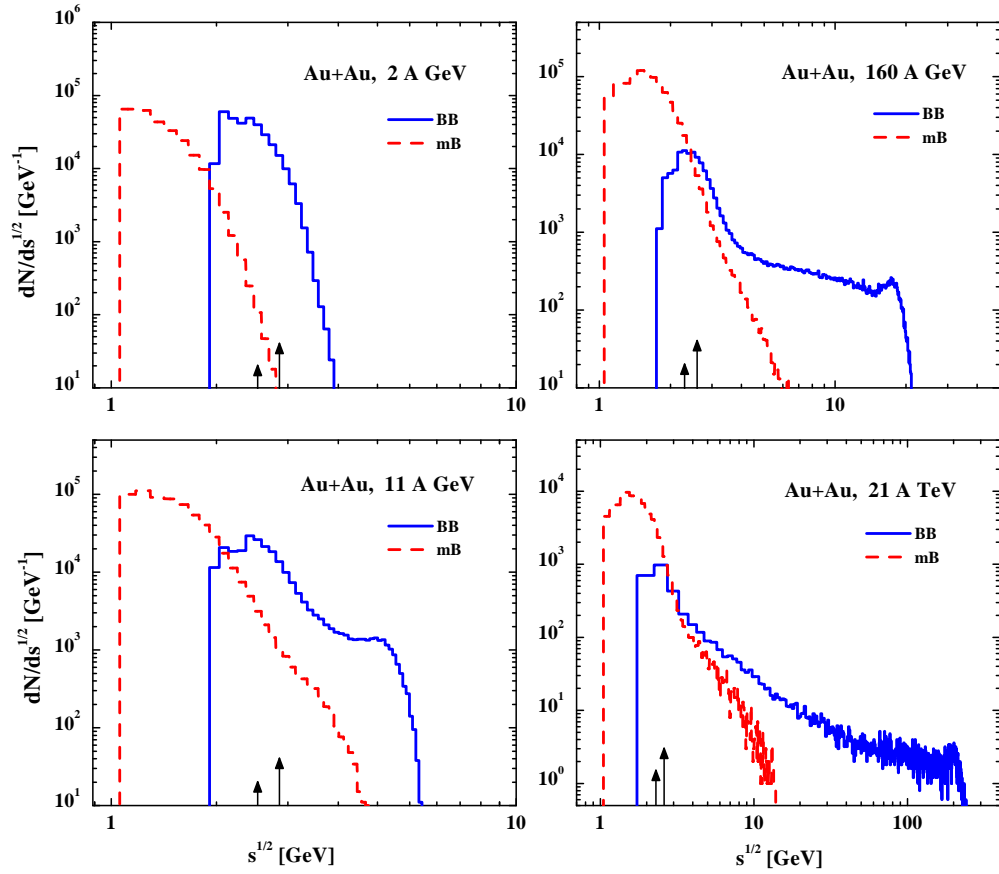


Figure 13: The number of baryon-baryon (solid histograms) and meson-baryon collisions (dashed histograms) as a function of the invariant energy \sqrt{s} for central ($b \leq 1.5$ fm) Au + Au collisions at bombarding energies of 2, 11, 160 A·GeV and 21 A·TeV, respectively, from the HSD model. The arrows indicate the string thresholds for mB and BB collisions of 2.3 GeV and 2.6 GeV, respectively.

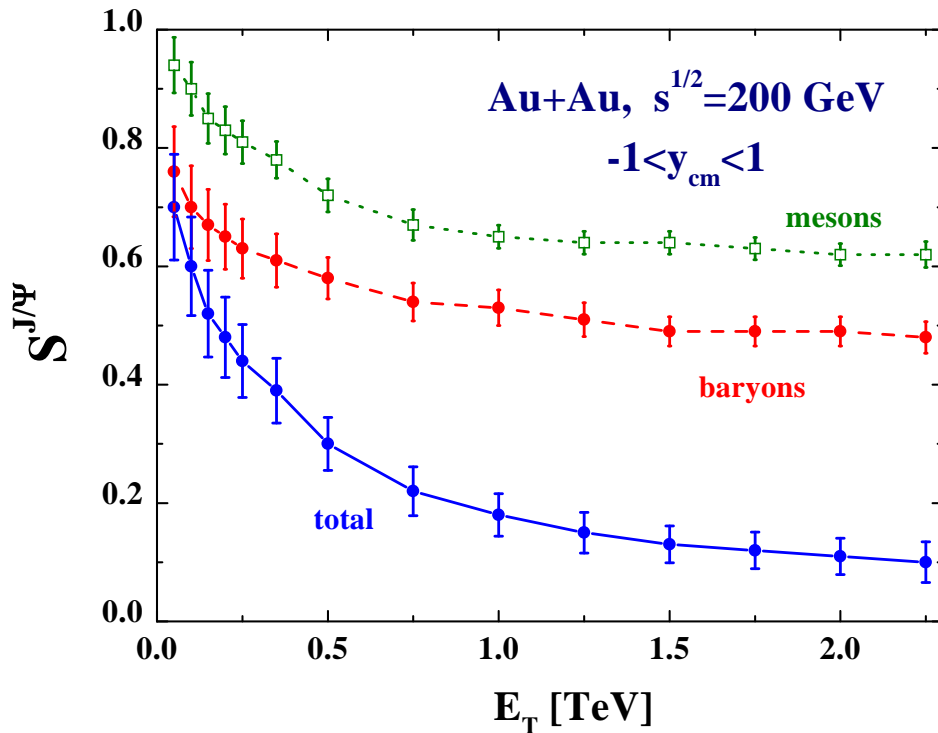


Figure 14: The J/Ψ survival factor $S_{J/\Psi}$ as a function of the transverse energy E_T in the rapidity interval ($-1 \leq y_{cm} \leq 1$) in Au + Au collisions at $\sqrt{s} = 200$ GeV in the 'late' comover model. The solid line represents the result for J/Ψ dissociation on nucleons and mesons, whereas the dashed line and the dotted line correspond to the absorption on baryons and mesons, respectively. The error bars in the figure are due to statistics only.